Frontiers of Information Technology & Electronic Engineering
www.jzus.zju.edu.cn; engineering.cae.cn; www.springerlink.com
ISSN 2095-9184 (print); ISSN 2095-9230 (online)
E-mail: jzus@zju.edu.cn

Accelerated haze removal for a single image by dark channel prior*

Bo-xuan YUE†, Kang-ling LIU, Zi-yang WANG, Jun LIANG†‡

State Key Laboratory of Industrial Control Technology, Zhejiang University, Hangzhou 310027, China

†E-mail: ybx90@outlook.com; jliang@iipc.zju.edu.cn

Received Feb. 27, 2017; Revision accepted Oct. 10, 2017; Crosschecked Aug. 15, 2019

Abstract: Haze scatters light transmitted in the air and reduces the visibility of images. Dealing with haze is still a challenge for image processing applications nowadays. For the purpose of haze removal, we propose an accelerated dehazing method based on single pixels. Unlike other methods based on regions, our method estimates the transmission map and atmospheric light for each pixel independently, so that all parameters can be evaluated in one traverse, which is a key to acceleration. Then, the transmission map is bilaterally filtered to restore the relationship between pixels. After restoration via the linear hazy model, the restored images are tuned to improve the contrast, value, and saturation, in particular to offset the intensity errors in different channels caused by the corresponding wavelengths. The experimental results demonstrate that the proposed dehazing method outperforms the state-of-the-art dehazing methods in terms of processing speed. Comparisons with other dehazing methods and quantitative criteria (peak signal-to-noise ratio, detectable marginal rate, and information entropy difference) are introduced to verify its performance.

Key words: Haze removal; Dark channel prior; Hazy image model; Bilateral filtering
https://doi.org/10.1631/FITEE.1700148 **CLC number:** TP751

1 Introduction

Computer vision methods are increasingly being applied in practice. Some current hotspots, such as automated driving systems (Magescas and Prablanc, 2006; Nebut et al., 2006; Karantzalos and Paragios, 2009; Yeo et al., 2009) and robotics (de Gregorio et al., 2016; Downey et al., 2016; Yang et al., 2016; Zhang and Parker, 2016), depend heavily on computer vision, especially for outdoor image processing. The visibility of images plays an extremely important role in these applications. The scenic environment is one of the key elements for imaging quality. Bad weather, such as fog or haze, degrades the visibility and leads to a loss of color, contrast, and saturation. It diminishes the distinctions between the objects and the background, and results in color shifts, which are the basis for image processing. To remove the effects of haze, numerous dehazing approaches have been developed to restore a scene's radiance, thereby extending the application of computer vision. Moreover, instantaneity is rapidly becoming a necessary component in the dehazing area due to the requirements of real-time computer vision applications.

Haze removal is highly desired; however, it is difficult to achieve, especially for a single image. First, the criterion of haze is ambiguous. In practice, the air atmosphere is not free of haze even on clear days. Besides, humans perceive the scene depth due to the existence of haze. Second, sunlight easily influences the estimation of atmospheric light. Finally, it is difficult to achieve scene depth from a single image, and a transmission map is related to the scene depth.

‡ Corresponding author
* Project supported by the National Natural Science Foundation of China (Nos. U1664264 and U1509203)
ORCID: Bo-xuan YUE, http://orcid.org/0000-0001-8038-9834

Two different methods have been provided for haze removal: polarization (Schechner et al., 2001, 2003; Shwartz et al., 2006) and three-dimensional (3D) information (Narasimhan and Nayar, 2000, 2002, 2003). Both methods require more than one image. However, images of the same scene from various perspectives are difficult to obtain, and they usually require special devices, which are not widely used in practice. To solve this problem, researchers have proposed different approaches to remove haze from a single image. Currently, haze removal has achieved significant progress, although it depends on the robust priors. Tan (2008) discovered that a haze-free image must have higher contrast compared with the input hazy image. With this discovery, Tan (2008) removed haze using the maximization of the local contrast. However, the restored images show over-dehazing and are not physically available. Fattal (2008) proposed an assumption that the transmission and surface shading are locally uncorrelated. Thus, the transmission can be estimated by independent component analysis (ICA). Fattal (2008)'s method gave impressive results, but much time was consumed for transmission map estimation by ICA. He et al. (2010) suggested the dark channel prior, where, in most of the local regions which do not cover the sky, some pixels always have very low intensity in at least one color channel (RGB). Hazy images were divided into small patches to generate the dark channel and a guided image filter was introduced to process the borders of each patch. He et al. (2010) provided a novel perspective for haze removal. Zhu et al. (2015) proposed a prior, called "a color attenuation prior," where the concentration of the haze was positively correlated with the difference between brightness and saturation (HSV), according to the statistics. Zhu et al. (2015) estimated the transmission map with a supervised learning method. This method is robust; however, it needs a database of hazy images. All of the above-mentioned research represents the explorations into dehazing and extends the trends in dehazing development.

In this study, we propose an accelerated haze removal method for a single image. Our approach is impressive in its rapidity. In this approach, it takes only one traversal to estimate the transmission map and atmospheric light. This is the key to the acceleration of haze removal. After the estimation, the image is restored based on the linear model of hazy images. Further post-processing helps improve the physical validity.

2 Background

2.1 Hazy image model

Haze is caused by visibility-reducing aerosols of the wet type, and leads to degradations in scene radiance and enhanced airlight. The hazy image model is generally given as (Koschmeider, 1924)

$$I(x) = J(x) \cdot t(x) + A[1 - t(x)], \tag{1}$$

where I is the observed intensity, J the scene radiance, t the medium transmission map describing the portion of the light that is not scattered and reaches the camera, and A the atmospheric light. The objective of haze removal is to restore J from I with t and A, which is the reason why haze removal for a single image is difficult.

In the linear model, $J(x)\cdot t(x)$ represents the direct attenuation, which indicates the scene radiance and its decay in the medium. $t(x)$ represents the airlight (Chavez, 1988), which is generated from the atmospheric light and leads to the shift in the scene radiance. When the atmosphere is homogenous, the transmission map t can be expressed as (Gilchrist and Jacobsen, 1983)

$$t(x) = \beta \mathrm{e}^{d(x)}, \tag{2}$$

where β is the scattering coefficient of the atmosphere and d the scene depth. Eq. (2) indicates that the scene radiance is exponentially attenuated with the depth. If the transmission is achieved, we can obtain the depth with an unknown coefficient.

2.2 Dark channel prior

The dark channel prior is based on the statistics of outdoor images. In most of the non-sky patches, at least one color channel has some pixels, whose intensities are very low and close to zero (He et al., 2010). For the input image, its dark channel $J_{\mathrm{dark}}(x)$ is expressed as

$$J_{\text{dark}}(x)=\min_{y\in\Omega(x)}\left[\min_{c\in\{\text{R,G,B}\}}J_c(y)\right], \tag{3}$$

where J_c is a color channel of J and $\Omega(x)$ a local patch centered at x. A dark channel is the outcome of two minimum operators: $\min_{y\in\Omega(x)}(\cdot)$ is performed on each pixel and $\min_{c\in\{\text{R,G,B}\}}(\cdot)$ on each channel. Given the aforementioned concept, if J is an outdoor haze-free image without sky regions, the intensity of the dark channel tends to zero:

$$J_{\text{dark}}(x)\to 0. \tag{4}$$

3 Accelerated method for haze removal

The proposed method for haze removal is composed mainly of four processes, extracting the dark channel, filtering the transmission map, restoring the hazy image, and tuning the color channels, and tends to remove the haze as fast as possible.

3.1 Dark channel extraction

As previously discussed, we extract the dark channel $J_{\text{dark}}(x)$ as Eq. (3). In particular, we compute the element-wise dark channel, and Eq. (3) can be simplified as

$$J_{\text{dark}}(x)=\min_{c\in\{\text{R,G,B}\}}J_c(x). \tag{5}$$

The size of the region $\Omega(x)$ determines the consumption time in achieving the dark channel. The simplification leads to achieving the dark channel in one single circulation, which makes it more than 20 times faster than conventional methods.

The most haze-opaque regions shown in Fig. 1 are generally used as the global atmospheric light, which are the points with the greatest scene depth. This region can have the highest intensity in the dark channel J_{dark}. The top 0.1% brightest pixels are selected as the most haze-opaque regions, and the average intensity of the region is our estimation for the global atmospheric light A.

Our estimation of the atmospheric light is to search for the maximum in the dark channel. However, the estimated atmospheric light $\bar{A}$ is a little higher than the actual value. To fix this overestimation, a correction based on statistics is introduced. Fig. 2 shows that the maxima are close to the mean of the top 0.1% brightest pixels. The real atmospheric light $\tilde{A}$ can be expressed as

$$\tilde{A}=\eta\bar{A}, \tag{6}$$

where η is the correction factor, taking the value in the range of 0.95 to 0.99 based on the statistics.

Fig. 1 The most haze-opaque regions for estimating the atmospheric light

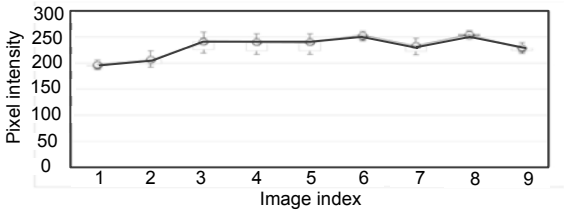

Fig. 2 Distribution of the maxima and averages of the top 0.1% hazy images

3.2 Transmission map filtering

We achieve the transmission map t with the assumption that the atmospheric light A is given. Normalizing the hazy image model, Eq. (1) can be presented as

$$\frac{I_c(x)}{A_c}=t(x)\cdot\frac{J_c(x)}{A_c}+\big(1-t(x)\big). \tag{7}$$

The transmission map t can be estimated according to the dark channel prior, i.e.,

$$J_{\text{dark}}(x)=\min_{c\in\{\text{R,G,B}\}}J_c(x)=0. \tag{8}$$

As A_c is positive real, the transmission map can be estimated as

$$\tilde{t}(x)=1-\min_{c\in\{\text{R,G,B}\}}J_c(x), \tag{9}$$

where $\min_{c\in\{\mathrm{R,G,B}\}} J_c(x)$ is the dark channel of the normalized hazy image. In addition, because haze leads to the scene depth, a very small amount should be preserved, and Eq. (9) is expressed as

$$\tilde{t}(x)=1-\omega \min_{c\in\{\mathrm{R,G,B}\}} J_c(x), \tag{10}$$

where ω is a constant and is application based, typically in the range of 0.90 to 0.95 in He et al. (2010). In our experiments, ω is fixed at 0.95.

The transmission map needs filters to eliminate the noises from the extraction of dark channels. Since the transmission map depends on the scene depth, the objects with the same depth are supposed to share the same media transmission. The estimated transmission map preserves the boundaries; however, it is interfered with by shadows. The shadows are generated as a dark region on the surface of the scene's objects, which can be considered as noises for the dark channel. The noisy dark channel is expressed as

$$J_{\mathrm{dark}}(x)=J_{\mathrm{dark}}^{\mathrm{src}}(x)+S(x), \tag{11}$$

where $J_{\mathrm{dark}}^{\mathrm{src}}(x)$ is the dark channel of the source and $S(x)$ the shadow. To eliminate all such influences and noises, we need an edge-preserving filter to refine the transmission map. The kernel of this filter needs to have the capabilities of both denoising and edge preservation. We have tried several kinds of filters, for instance, bilateral filters (Tomasi and Manduchi, 1998), guided filters (He et al., 2013), and a domain transform (DT) filter (Gastal and Oliveira, 2011). All of them can achieve good performances.

3.3 Hazy image restoration

With the atmospheric light and the transmission map being achieved, the scene radiance can be restored according to Eq. (1). However, the transmission map can be close to zero, which can result in noises in the restored images. Hence, a restriction t_0 is used to forbid the estimated media transmission $t(x)$, which is too small. In addition, the atmospheric light can shift colors when its intensity is high enough. We restrict the atmospheric light as $\tilde{A}$ by a higher restriction A_0. The restrictions are set to preserve the visibility in the very dense haze regions. Thus, the final scene radiance $J(x)$ is recovered by

$$J(x)=\frac{I(x)-\min(\tilde{A},A_0)}{\max\left(\tilde{t}(x),t_0\right)}+\min(\tilde{A},A_0), \tag{12}$$

where t_0 and A_0 are application based and their typical values are set as 0.1 and 240, respectively.

3.4 Color channel tuning

After the dehaze procedures being proposed, the hazy images are restored. Some works tend to enhance the dehazed images by color correction algorithms (Li and Guo, 2015), such as color compensation and histogram equalization. These algorithms are capable of providing a good contrast, resulting in color distortion. To improve the restoration, we propose an adjustment for different color channels according to different wavelengths.

In a hazy scene, the light decaying through the air suffers from different impacts of various wavelengths. It is aerosols that cause the generation of haze or fog, which reflects and refracts light. An aerosol is considered a colloidal system of solid or liquid particles in a gas, and the liquid or solid particles have a diameter most of which is smaller than 1 μm or so. Therefore, yellow light and red light have the best penetration in haze, because their specific wavelengths mean that the light can travel around the solid or liquid particles. With the assumption that the haze is homogenous, the transmission t can be reformed as

$$t(x)=\delta(\lambda)\beta \mathrm{e}^{d(x)}, \tag{13}$$

where $\delta(\lambda)$ is the normalized residual energy ratio (Li and Guo, 2015) based on the wavelength λ.

In the RGB space, different colors are regularized in three channels. According to different wavelengths, different channels of light differently decay. Hence, the transmission map should be presented as

$$t(x)=\left\{t_c(x)=\delta(\lambda_c)\beta \mathrm{e}^{d(x)} \mid c\in\{\mathrm{R,G,B}\}\right\}, \tag{14}$$

where $t_c(x)$ is the transmission map for different channels. According to the BSDS500 statistics (Arbelaez et al., 2011) and the refractive index equation, the normalized residual energy ratio $\delta(\lambda_c)$ can be expressed as

$$\delta(\lambda_c)=\begin{cases}0.80-0.85, & c=\mathrm{R},\\ 0.93-0.97, & c=\mathrm{G},\\ 0.95-0.99, & c=\mathrm{B}.\end{cases} \quad (15)$$

Thus, a hazy image is restored per channel, expressed as

$$J_c(x)=\frac{I(x)-\min(\tilde{A},A_0)}{\max\left(\tilde{t}_c(x),t_0\right)}+\min(\tilde{A},A_0). \quad (16)$$

4 Experimental results

To verify the performance of haze removal in the proposed approach, the tests covered the following three aspects: algorithmic complexity, dehazing effect, and quantitative analysis. The experimental results were compared with those of the existing dehazing algorithms.

4.1 Algorithmic complexity

The proposed approach is composed of three steps: estimating parameters, restoring images, and post-processing. It outperforms the dehaze methods in terms of speed because the atmospheric light and the transmission map are achieved in a single circulation. Given a hazy image with a size of $n=h\times w$, the algorithmic complexity in estimating the parameters is $O(n)$, which is as algorithmically complex as He et al. (2010)'s haze removal, which also uses the dark channel prior. He et al. (2010) used a window sized 15×15; in contrast, our approach runs by pixels instead of regions, and is about 20 times faster than He et al. (2010)'s approach in the first step.

Table 1 shows the comparison of computation time among our approach and other methods. The experiments were run on a laptop computer with Intel (Haswell) Core i5 CPU@1.9 GHz without GPU acceleration. The proposed method is much faster than the state-of-the-art methods. The good performance of our approach benefits mainly from the novel estimation of the atmospheric light and the transmission map.

4.2 Dehazing effect

Each algorithm can achieve scene radiance; however, it is difficult to evaluate it without the original hazy images. We demonstrate some results to show the efficiency of the proposed methods. Moreover, to illustrate visual quality, some other classical algorithms are compared with our methods.

Fig. 3 shows a set of our experimental results, which are comparisons between the hazy images and the restored images. We used a bilateral filter to smooth the transmission map, which was set at a window width of eight, and the variance of space and the variance of color were both 30. The hazy images were collected from Fattal (2014). The results show that our method can remove haze well.

Figs. 4 and 5 show our results and those obtained with five dehazing algorithms. To affirm the effects, we also show the results for Canny detection. Furthermore, Figs. 4 and 5 show the situations for thin and dense haze, respectively. In Fig. 4, the images with thin haze are refined well by different methods. Fattal (2008)'s results in Fig. 4b and He et al. (2010)'s results in Fig. 4c seem dark. Nishino et al. (2012)'s results in Fig. 4d show the least edges, and it lacks a capacity to improve contrast. Gibson and Nguyen (2013)'s results in Fig. 4e give the most edges. Because our results are tuned according to different wavelengths, the proposed method enriches the image on a color display.

Fig. 5 shows the results in a dense-haze situation. All the methods restore the foreground well. Berman et al. (2016)'s method improves the contrast of most of the five methods in Fig. 5f. He et al. (2010)'s output images in Fig. 5c are still darker than others. Our results have the least purple fringe, compared with other results.

4.3 Quantitative analysis

It is a challenge to evaluate the image quality, especially when the original radiance cannot be achieved. To analyze the proposed method, we introduced three performance indexes: peak signal-to-noise ratio (PSNR), detectable marginal rate (DMR), and information entropy difference (IED).

PSNR is a most commonly used metric to measure the quality of reconstruction in lossy compression. It is introduced in this study to describe how much the input images are transformed. PSNR is defined via the mean squared error (MSE), expressed as

$$\mathrm{MSE}=\frac{1}{3N}\sum_{n=0}^{N}\sum_{c\in\{\mathrm{R,G,B}\}}\|\boldsymbol{I}_c(n)-\boldsymbol{J}_c(n)\|^2, \quad (17)$$

Table 1 Comparison of consumption time among the methods proposed by Fattal (2008), He et al. (2010), Gibson and Nguyen (2013), Berman et al. (2016) and our method

Image resolution	Consumption time (s)				
	Fattal (2008)	He et al. (2010)	Gibson and Nguyen (2013)	Berman et al. (2016)	This paper
293×220	2.872	1.066	1.664	1.738	0.232
600×450	11.825	4.929	7.776	8.022	0.981
800×600	21.343	7.503	13.967	14.466	1.764
1080×720	34.537	12.005	21.101	35.288	2.882
1920×1080	90.118	33.913	49.009	53.077	7.519

Fig. 3 Comparison of hazy images with restored images

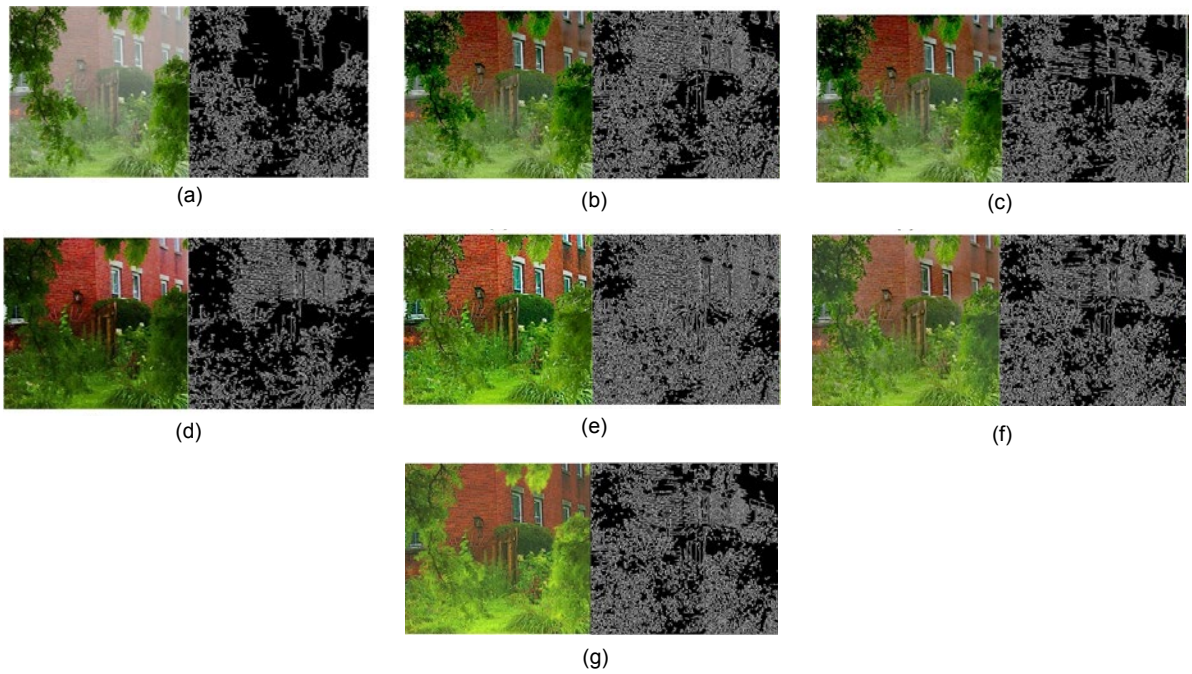

Fig. 4 Comparison of the proposed approach with the existing methods: (a) input images with thin haze; (b) Fattal (2008)'s method; (c) He et al. (2010)'s method; (d) Nishino et al. (2012)'s method; (e) Gibson and Nguyen (2013)'s method; (f) Berman et al. (2016)'s method; (g) our method

The right part of each subfigure represents the corresponding results for the Canny edge detector

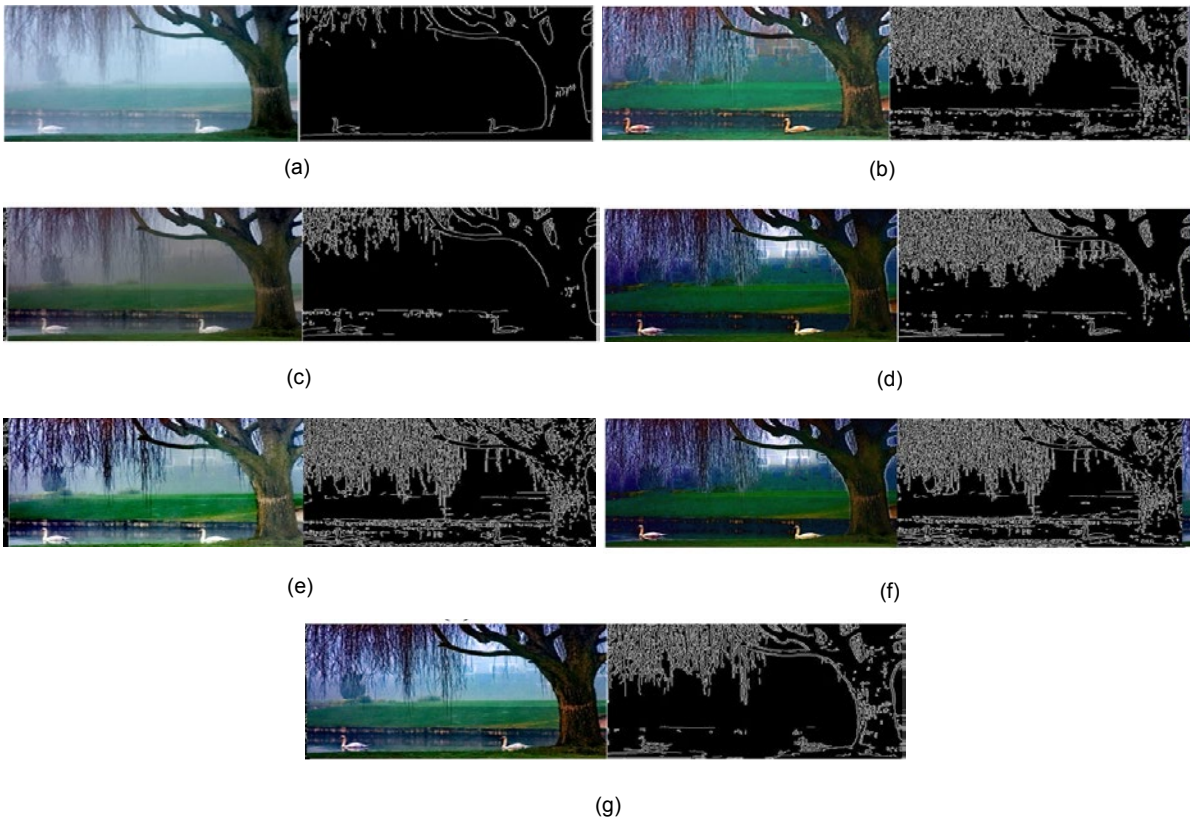

Fig. 5 Comparison of the proposed approach with the existing methods: (a) input images with dense haze; (b) Fattal (2008)'s method; (c) He et al. (2010)'s method; (d) Nishino et al. (2012)'s method; (e) Gibson and Nguyen (2013)'s method; (f) Berman et al. (2016)'s method; (g) our method

The right part of each subfigure represents the corresponding results for the Canny edge detector. References to color refer to the online version of this figure

where $\boldsymbol{I}$ is the observed intensity, $\boldsymbol{J}$ the scene radiance, and N the number of pixels within image $\boldsymbol{I}$. Thus, PSNR (in dB) is defined as

$$\mathrm{PSNR}=10\lg\frac{\max_I^2}{\mathrm{MSE}}, \tag{18}$$

where $\max_I$ is the maximum possible pixel value of the image with the default value of 255. A low PSNR indicates that the method greatly transforms the image.

Table 2 shows the comparison of MSE and PSNR among different methods. It can be seen that Berman et al. (2016)'s method gave the lowest PSNR and the highest MSE, which describes how this method most changes the hazy images. In contrast, Gibson and Nguyen (2013)'s method provides the highest PSNRs of all. Our method achieves different PSNRs because the different images have different haze densities.

The marginal rate is defined as the difference in the edges between the hazy and dehazed images. The Canny edge detector (Deriche, 1987) determines the edges. Thus, the DMR r is expressed as

$$r_x=\mathrm{Canny}(I_x)/\mathrm{size}(I_x), \tag{19}$$

where Canny(·) represents the Canny edge detector and size(·) the operator to compute the number of elements in a matrix. The DMR describes the number of the edges that can be detected. The difference in DMR between the input hazy images and the output dehazed images, Δr, presents the change in the number of detectable edges, expressed as

$$\Delta r=r_{\mathrm{dehazed}}-r_{\mathrm{hazy}}. \tag{20}$$

A high DMR difference shows that no matter how many improvements are made to promote object visibility in the image, they are not distinct from the

background. Achievement of a high DMR is the original purpose of haze removal.

From Table 3, the proposed method provides a positive DMR in images 1, 2, and 3, which means that it provides more detectable edges. Gibson and Nguyen (2013)'s method supplies the highest Δr, while He et al. (2010)'s method gives the lowest one. Our method works well on images 1 and 2, but not that well on image 3, because image 3 describes a dense-haze scene. However, as a method based on dark channel prior (DCP), our method achieves great progress compared with He et al. (2010)'s method.

According to our previous discussion, hazy images lose information because of the haze. Hence, we introduce information entropy as estimation for dehazing efficacy, especially in the color space. The IED is defined as the difference between the entropies of the hazy and dehazed images, which is the expected value of the information contained in each image. A high entropy indicates that the image contains considerable information in the color space.

The information entropy can be described as

$$E(x) = -\sum_{i=1}^{n} P(x_i) \log_2 P(x_i), \tag{21}$$

where $P(x_i)$ is the probability mass function and x_i the discrete color value. The IED is represented as

$$\Delta e = E_{\text{dehazed}} - E_{\text{hazy}}. \tag{22}$$

This difference shows the improvement in the hazy images in the color space by the methods.

Table 4 shows that all the methods can raise the information entropy. Obviously, our method can achieve a high IED for different images, while all the methods provide various IEDs for different images. This affirms the performance of our method.

After computational complexity and quantitative analysis, the proposed method can effectively remove haze at an impressively high speed.

5 Conclusions

In this paper, we have proposed an approach to remove haze for a single image. The transmission map and atmospheric light are achieved in a single circulation. A bilateral filter has been used to refine the transmission map. The atmospheric light has been corrected by experience and the statistics

Table 2 MSE and PSNR comparison among the methods proposed by Fattal (2008), He et al. (2010), Nishino et al. (2012), Gibson and Nguyen (2013), Berman et al. (2016) and our method

Method	MSE			PSNR (dB)		
	Image 1	Image 2	Image 3	Image 1	Image 2	Image 3
Fattal (2008)'s	99.35	108.35	103.36	8.218	7.4344	7.874
He et al. (2010)'s	107.26	105.45	104.82	7.543	7.670	7.772
Nishino et al. (2012)'s	105.45	103.19	100.22	7.707	7.858	8.112
Gibson and Nguyen (2013)'s	96.36	100.85	102.89	8.485	8.057	7.883
Berman et al. (2016)'s	105.85	109.43	109.04	7.706	7.348	7.379
Ours	107.78	101.82	94.824	7.543	7.975	8.642

Table 3 Differences in detectable marginal rates of the methods proposed by Fattal (2008), He et al. (2010), Nishino et al. (2012), Gibson and Nguyen (2013), Berman et al. (2016) and our method

Method	r_{hazy}			Δr		
	Image 1	Image 2	Image 3	Image 1	Image 2	Image 3
Fattal (2008)'s	39.195	30.558	10.103	23.436	30.832	33.672
He et al. (2010)'s	39.195	30.558	10.103	12.648	27.596	4.930
Nishino et al. (2012)'s	39.195	30.558	10.103	6.059	36.184	24.299
Gibson and Nguyen (2013)'s	39.195	30.558	10.103	37.781	34.658	35.871
Berman et al. (2016)'s	39.195	30.558	10.103	20.926	33.900	38.837
Ours	39.195	30.558	10.103	30.651	32.744	26.510

Table 4 Information entropy differences of the methods proposed by Fattal (2008), He et al. (2010), Nishino et al. (2012), Gibson and Nguyen (2013), Berman et al. (2016) and our method

Method	Information entropy difference		
	Image 1	Image 2	Image 3
Fattal (2008)'s	0.004	0.152	0.369
He et al. (2010)'s	0.100	0.297	0.402
Nishino et al. (2012)'s	0.206	0.393	0.610
Gibson and Nguyen (2013)'s	0.140	0.374	0.440
Berman et al. (2016)'s	0.355	0.147	0.046
Ours	0.228	0.281	0.421

to constrain the overestimation. We have restored the images by the channels based on different wavelengths. To evaluate the performance of this approach, our method has been compared with the existing dehazing algorithms. The experimental results show that the proposed algorithm outperforms other methods in terms of efficiency and dehazing effects.

Compliance with ethics guidelines

Bo-xuan YUE, Kang-ling LIU, Zi-yang WANG, and Jun LIANG declare that they have no conflict of interest.

References

Arbelaez P, Maire M, Fowlkes C, et al., 2011. Contour detection and hierarchical image segmentation. *IEEE Trans Patt Anal Mach Intell*, 33(5):898-916. https://doi.org/10.1109/TPAMI.2010.161

Berman D, Treibitz T, Avidan S, 2016. Non-local image dehazing. IEEE Conf on Computer Vision and Pattern Recognition, p.1674-1682. https://doi.org/10.1109/CVPR.2016.185

Chavez PSJr, 1988. An improved dark-object subtraction technique for atmospheric scattering correction of multispectral data. *Remote Sens Environ*, 24(3):459-479. https://doi.org/10.1016/0034-4257(88)90019-3

de Gregorio M, Giordano M, Rossi S, et al., 2016. Experimenting WNN support in object tracking systems. *Neurocomputing*, 183:79-89. https://doi.org/10.1016/j.neucom.2015.09.117

Deriche R, 1987. Using Canny's criteria to derive a recursively implemented optimal edge detector. *Int J Comput Vis*, 1(2):167-187. https://doi.org/10.1007/bf00123164

Downey JE, Weiss JM, Muelling K, et al., 2016. Blending of brain-machine interface and vision-guided autonomous robotics improves neuroprosthetic arm performance during grasping. *J Neuroeng Rehabil*, 13, Article 28. https://doi.org/10.1186/s12984-016-0134-9

Fattal R, 2008. Single image dehazing. *ACM Trans Graph*, 27(3), Article 72. https://doi.org/10.1145/1360612.1360671

Fattal R, 2014. Dehazing using color-lines. *ACM Trans Graph*, 34(1), Article 13. https://doi.org/10.1145/2651362

Gastal ESL, Oliveira MM, 2011. Domain transform for edge-aware image and video processing. *ACM Trans Graph*, 30(4):1-12. https://doi.org/10.1145/1964921.1964964

Gibson KB, Nguyen TQ, 2013. An analysis of single image defogging methods using a color ellipsoid framework. *EURASIP J Image Video Process*, 2013:37. https://doi.org/10.1186/1687-5281-2013-37

Gilchrist AL, Jacobsen A, 1983. Lightness constancy through a veiling luminance. *J Exp Psychol Hum Perc Perform*, 9(6):936-944. https://doi.org/10.1037/0096-1523.9.6.936

He K, Jian S, Tang X, 2010. Single image haze removal using dark channel prior. *IEEE Trans Patt Anal Mach Intell*, 33(12):2341-2353. https://doi.org/10.1109/TPAMI.2010.168

He K, Sun J, Tang X, 2013. Guided image filtering. *IEEE Trans Patt Anal Mach Intell*, 35(6):1397-1409. https://doi.org/10.1109/TPAMI.2012.213

Karantzalos K, Paragios N, 2009. Recognition-driven two-dimensional competing priors toward automatic and accurate building detection. *IEEE Trans Geosci Remote Sens*, 47(1):133-144. https://doi.org/10.1109/tgrs.2008.2002027

Koschmeider H, 1924. Theorie der horizontalen sichtweite. *Beitr Phys Freien Atmosph*, 12:33-53, 171-181 (in German).

Li CY, Guo JC, 2015. Underwater image enhancement by dehazing and color correction. *J Electron Imag*, 24(3): 033023. https://doi.org/10.1117/1.jei.24.3.033023

Magescas F, Prablanc C, 2006. Automatic drive of limb motor plasticity. *J Cogn Neurosci*, 18(1):75-83. https://doi.org/10.1162/089892906775250058

Narasimhan SG, Nayar SK, 2000. Chromatic framework for vision in bad weather. IEEE Computer Society Conf on Computer Vision and Pattern Recognition, p.1-8.

Narasimhan SG, Nayar SK, 2002. Vision and the atmosphere. *Int J Comput Vis*, 48(3):233-254.

Narasimhan SG, Nayar SK, 2003. Contrast restoration of weather degraded images. *IEEE Trans Patt Anal Mach Intell*, 25(6):713-724. https://doi.org/10.1109/TPAMI.2003.1201821

Nebut C, Fleurey F, Le Traon Y, et al., 2006. Automatic test generation: a use case driven approach. *IEEE Trans Softw Eng*, 32(3):140-155. https://doi.org/10.1109/tse.2006.22

Nishino K, Kratz L, Lombardi S, 2012. Bayesian defogging. *Int J Comput Vis*, 98(3):263-278. https://doi.org/10.1007/s11263-011-0508-1

Schechner YY, Narasimhan SG, Nayar SK, 2001. Instant dehazing of images using polarization. Proc IEEE Conf on Computer Vision and Pattern Recognition, p.1-8. https://doi.org/10.1109/CVPR.2001.990493

Schechner YY, Narasimhan SG, Nayar SK, 2003. Polarization-based vision through haze. *Appl Opt*, 42(3): 511-525.

Shwartz S, Namer E, Schechner YY, 2006. Blind haze separation. IEEE Computer Society Conf on Computer Vision and Pattern Recognition, p.1-8.

Tan RT, 2008. Visibility in bad weather from a single image. IEEE Computer Society Conf on Computer Vision and Pattern Recognition, p.1-8.

Tomasi C, Manduchi R, 1998. Bilateral filtering for gray and color images. Proc IEEE Int Conf on Computer Vision, p.1-8.

Yang Y, Song YT, Pan HT, et al., 2016. Visual servo simulation of EAST articulated maintenance arm robot. *Fus Eng Des*, 104:28-33. https://doi.org/10.1016/j.fusengdes.2016.01.024

Yeo MVM, Li XP, Shen KQ, et al., 2009. Can SVM be used for automatic EEG detection of drowsiness during car driving? *Saf Sci*, 47(1):115-124. https://doi.org/10.1016/j.ssci.2008.01.007

Zhang H, Parker LE, 2016. CoDe4D: color-depth local spatio-temporal features for human activity recognition from RGB-D videos. *IEEE Trans Circ Syst Video Technol*, 26(3):541-555. https://doi.org/10.1109/tcsvt.2014.2376139

Zhu QS, Mai JM, Shao L, 2015. A fast single image haze removal algorithm using color attenuation prior. *IEEE Trans Image Process*, 24(11):3522-3533. https://doi.org/10.1109/tip.2015.2446191